

Enhancement of four-wave mixing due to coherent hole burning in a degenerate two-level system

Zhi-Yuan Liu(刘知远), Yi-Fan Yao(姚一凡), Yue Sun(孙悦), Jia-Yu Han(韩佳瑜), and Ying-Jie Du(杜英杰)
Citation: Chin. Phys. B, 2025, 34 (**5**): 054203. DOI: 10.1088/1674-1056/adb949
http://cpb.iphy.ac.cn; http://iopscience.iop.org/cpb

What follows is a list of articles you may be interested in

Four-wave mixing Bragg scattering for small frequency shift from silicon coupled microrings

Chang Zhao(赵畅), Chao Wu(吴超), Pingyu Zhu(朱枰谕), Yuxing Du(杜昱星), Yan Wang(王焱), Miaomiao Yu(余苗苗), Kaikai Zhang(张凯凯), and Ping Xu(徐平)
Chin. Phys. B, 2025, 34 (**1**): 014206. DOI: 10.1088/1674-1056/ad8a4f

Intrinsic polarization conversion and avoided-mode crossing in X-cut lithium niobate microrings

Zelin Tan(谭泽林), Jianfa Zhang(张检发), Zhihong Zhu(朱志宏), Wei Chen(陈伟), Zhengzheng Shao(邵铮铮), Ken Liu(刘肯), and Shiqiao Qin(秦石乔)
Chin. Phys. B, 2024, 33 (**6**): 064205. DOI: 10.1088/1674-1056/ad47b2

Effects of cross-Kerr coupling on transmission spectrum of double-cavity optomechanical system

Li-Teng Chen(陈立滕), Li-Guo Qin(秦立国), Li-Jun Tian(田立君), Jie-Hui Huang(黄接辉), Nan-Run Zhou(周南润), and Shang-Qing Gong(龚尚庆)
Chin. Phys. B, 2024, 33 (**6**): 064204. DOI: 10.1088/1674-1056/ad2507

Effectively modulating spatial vortex four-wave mixing in a diamond atomic system

Nuo Ba(巴诺), Ming-Qi Jiang(姜明奇), Jin-You Fei(费金友), Dan Wang(王丹), Hai-Lin Jiang(蒋海林), Lei Wang(王磊), and Hai-Hua Wang(王海华)
Chin. Phys. B, 2024, 33 (**4**): 044202. DOI: 10.1088/1674-1056/ad0771

Generation of mid-infrared supercontinuum by designing circular photonic crystal fiber

Ying Huang(黄颖), Hua Yang(杨华), and Yucheng Mao(毛雨澄)
Chin. Phys. B, 2022, 31 (**5**): 054211. DOI: 10.1088/1674-1056/ac272c

---

Enhancement of four-wave mixing due to coherent hole burning in a degenerate two-level system

Zhi-Yuan Liu(刘知远)[1], Yi-Fan Yao(姚一凡)[1], Yue Sun(孙悦)[1], Jia-Yu Han(韩佳瑜)[1], and Ying-Jie Du(杜英杰)[1,2,†]

[1] *School of Physics, Northwest University, Xi'an* 710127, *China*
[2] *Collaborative Innovation Center of Extreme Optics, Shanxi University, Taiyuan* 030006, *China*

(Received 19 November 2024; revised manuscript received 12 January 2025; accepted manuscript online 24 February 2025)

We present a theoretical study of four-wave mixing (FWM) in a degenerate two-level atomic system subject to a magnetic field whose Zeeman sublevels constitute a tripod-type atomic system, which is driven by a linearly polarized field, and coupled and probed by two sets of left and right circularly polarized fields. The optical effects of coherent hole burning (CHB) and electromagnetically induced transparency (EIT) are involved in the coherent system, among which the CHB has much larger response for the FWM than the EITs. Three situations of CHB are involved, and they are the solitary CHB, overlapped CHBs, and an overlap between CHB and EIT. The overlapped CHBs have the greatest magnitude of FWM signal among the three situations. Whereas, for the overlapped CHB and EIT, it has the smallest FWM magnitude, which is no more than one tenth of the former. While for the single CHB, the FWM magnitude is half of that of the overlapped CHBs. It is noted that, in the overlap between CHB and EIT, dual EIAs can be obtained, whose FWM signal also has an enhancement in comparison to no EIA.

Keywords: four-wave mixing, coherent hole burning, electromagnetically induced transparency, electromagnetically induced absorption

PACS: 42.50.Gy, 32.80.QK, 42.65.–K

DOI: 10.1088/1674-1056/adb949 **CSTR:** 32038.14.CPB.adb949

1. Introduction

Four-wave mixing (FWM) is a third-order nonlinear optical effect, which has extensive applications in the domains of optics, laser technology, quantum information, communication, etc. In the optics domain, FWM can be utilized to generate multiple femtosecond laser pulses with different central wavelengths, and expand the application scope of laser sources.[1–3] In the laser domain, FWM offers a new approach to the purification and stability of seed sources, and promotes ultra-strong and ultra-short laser technologies.[4,5] This is of great significance in applications requiring powerful lasers, such as laser nuclear fusion and high-energy physics research. In the domain of quantum information, technology based on FWM can realize quantum squeezing enhancement and quantum entangled states,[6–8] which has significant potential application in fields such as quantum computing,[9,10] quantum communication[11,12] and quantum precision measurement.[13,14] However, the FWM signal is generally weak and its occurrence is often accompanied by the use of powerful light. Fortunately, highly efficient FWM can be achieved with weak light under quantum coherence, which is generated in multiple atom–light systems.

The interaction between multifield and multilevel systems in a degenerate two-level system is a mixture of pure two-level systems, three-level systems and even N-type four-level systems. The pure two-level system is linked to Mollow absorption and coherent hole burning (CHB).[15,16] The three-level system is related to two-photon resonance, which can lead to electromagnetically induced transparency (EIT),[17–19] coherent population trapping (CPT)[20–22] and so on. The N-type four-level system is not only associated with two-photon resonance, but also with electromagnetically induced absorption (EIA).[23,24] The effect of CHB is related to coherent population oscillation, which is induced by coupled and probe fields in a pure two-level system.[25,26] Although CHB and EIT have similar performance in the absorption spectra, the dip of the CHB can be converted to emission from absorption, while EIT cannot realize it. On the other hand, CHB and EIT both involve the transfer of populations.[27] The population transfer in EIT happens in at least three-level atomic systems.[28–30] However, the population transfer in CHB mainly occurs in two-level systems, where the populations coherently oscillate between lower and upper levels.[29] This difference leads to obvious differences in the nonlinear responses.

In the past decades, the nonlinear effects of EIT have been extensively investigated[31–35] and the FWM response of CHB has also been investigated.[24,36] A three-peaked FWM spectrum in a pure two-level system was achieved by Boyed *et al.*[24] Subsequently, the multi-peaked structure of FWM was obtained and explained as the resonant emission between 'vir-

†Corresponding author. E-mail: yingjied@nwu.edu.cn

© 2025 Chinese Physical Society and IOP Publishing Ltd. All rights, including for text and data mining, AI training, and similar technologies, are reserved.

tual states' in the dressed picture by Sun *et al.*[36] However, CHB–CHB and CHB–EIT interactions have seldom been explored. Indeed, these interactions could modify the magnitude of the FWM signal and they can be adjusted by the detuned coupled fields. In this case, the CHB–CHB and CHB–EIT interactions can be achieved in the degenerate two-level system. It indicates that the enhanced FWM can be obtained by means of the interaction between CHB. In this paper, we present a theoretical study of the FWM spectra in a degenerate two-level atomic system whose Zeeman sublevels construct a tripod-type system under a magnetic field, which is driven by a linearly polarized field and coupled and probed by two sets of circularly polarized fields. With this multilevel system, the optical effects of CHB, EIT and EIA are included in the complex atom–light system. Among these effects, the CHB plays a critical role in the high quantum efficiency of FWM. The different states for the CHB are obtained by the manipulation of coupled detunings. The overlapped CHBs have the largest FWM response of the FWM signal while the overlapped EIT and CHB have the minimum response, about one tenth of the former, and between them is the state of a single CHB whose FWM magnitude is one half of the former. In the last case, double EIAs with subnatural-linewidth absorptions can be achieved in the state of overlapped EIT and CHB, whose FWM spectra exhibit four peaks with their magnitudes being enhanced.

2. Model and density matrix equations

Consider the simplest degenerate two-level system with the upper level $F_e = 0$ and the lower level $F_g = 1$. Under an applied magnetic field, the upper level of the degenerate two-level system remains, whereas the lower level splits into three hyperfine levels, each separated by equal energy gaps, which are related to the static magnetic field of strength B and satisfy $\omega_{21} = \omega_{32} = g\mu_B B/\hbar$, where g is the Lande factor and μ_B is the Bohr magneton. The configuration of the atomic system is shown in Fig. 1. The transition $|2\rangle$–$|4\rangle$ is driven by a linearly polarized field ω_2 with Rabi frequency V_2. The transitions $|1\rangle$–$|4\rangle$ and $|3\rangle$–$|4\rangle$ are coupled by two different circular polarized fields, ω_1 and ω_3 of $\sigma_\pm$, with Rabi frequencies V_1 and V_3, respectively. Meanwhile, the transitions $|1\rangle$–$|4\rangle$ and $|3\rangle$–$|4\rangle$ are monitored by two probe fields ω_{p_1} and ω_{p_2}, with Rabi frequencies V_{p_1} and V_{p_2}, respectively. Here the decay of atomic energy levels caused by spontaneous emission and the exchange of population between the ground state levels due to collisions are considered. The detunings of the coupled field V_1, driving field V_2 and coupled field V_3 are Δ_1, Δ_2 and Δ_3, respectively, which are defined by $\Delta_1 = \omega_1 - \omega_{41}$, $\Delta_2 = \omega_2 - \omega_{42}$ and $\Delta_3 = \omega_3 - \omega_{43}$. All transitions have dipole moments of the same magnitude but different symbols, $\mu_{41} = \mu_{43} = -\mu_{42} = \mu$. This degenerate system can be implemented in Sm,[37,38] Ne*,[39] and ^{87}Rb[40] atoms.

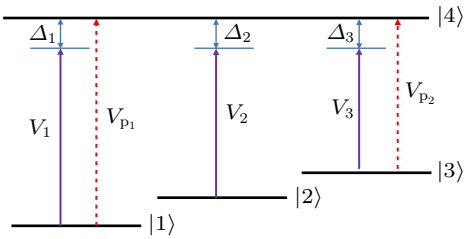


Fig. 1. Diagram of the levels for a degenerate two-level system $F_e = 0 \leftrightarrow F_g = 1$. It is driven by a linear polarized field with Rabi frequency V_2, coupled by two different circularly polarized fields with Rabi frequencies V_1 and V_3, respectively, and monitored by two probe fields with Rabi frequencies V_{p_1} and V_{p_2}, respectively. The detunings of the coupled fields are Δ_1 and Δ_3, respectively.

Under the rotating-wave and dipole approximations, the optical Bloch equations of the system are given by

$$\begin{aligned}
\dot{\rho_{11}} &= -\mathrm{i}\,(V_1\rho_{14} - \rho_{41}V_1^*) - (\Gamma_{12}+\Gamma_{13})\,\rho_{11} \\
&\quad +\Gamma_{41}\rho_{44} + \Gamma_{21}\rho_{22} + \Gamma_{31}\rho_{33}, && (1)\\
\dot{\rho_{22}} &= -\mathrm{i}\,(V_2\rho_{24} - \rho_{42}V_2^*) - (\Gamma_{21}+\Gamma_{23})\,\rho_{22} \\
&\quad +\Gamma_{42}\rho_{44} + \Gamma_{12}\rho_{11} + \Gamma_{32}\rho_{33}, && (2)\\
\dot{\rho_{33}} &= -\mathrm{i}\,(V_3\rho_{34} - \rho_{43}V_3^*) - (\Gamma_{32}+\Gamma_{31})\,\rho_{33} \\
&\quad +\Gamma_{43}\rho_{44} + \Gamma_{23}\rho_{22} + \Gamma_{13}\rho_{11}, && (3)\\
\dot{\rho_{44}} &= \mathrm{i}\,(V_1\rho_{14} - \rho_{41}V_1^*) + \mathrm{i}\,(V_3\rho_{34} - \rho_{43}V_3^*) \\
&\quad +\mathrm{i}\,(V_2\rho_{24} - \rho_{42}V_2^*) - (\Gamma_{41}+\Gamma_{43}+\Gamma_{42})\,\rho_{44}, && (4)\\
\dot{\rho_{41}} &= -\mathrm{i}[V_1(\rho_{44}-\rho_{11}) - V_3\rho_{31} - V_2\rho_{21}] \\
&\quad -(\mathrm{i}\omega_{41}+\gamma_{41})\rho_{41}, && (5)\\
\dot{\rho_{42}} &= -\mathrm{i}[V_2(\rho_{44}-\rho_{22}) - V_1\rho_{12} - V_3\rho_{32}] \\
&\quad -(\mathrm{i}\omega_{42}+\gamma_{42})\rho_{42}, && (6)\\
\dot{\rho_{43}} &= -\mathrm{i}[V_3(\rho_{44}-\rho_{33}) - V_1\rho_{13} - V_2\rho_{23}] \\
&\quad -(\mathrm{i}\omega_{43}+\gamma_{43})\rho_{43}, && (7)\\
\dot{\rho_{31}} &= -\mathrm{i}\,(V_1\rho_{34} - \rho_{41}V_3^*) - (\mathrm{i}\omega_{31}+\gamma_{31})\rho_{31}, && (8)\\
\dot{\rho_{32}} &= -\mathrm{i}\,(V_2\rho_{34} - \rho_{42}V_3^*) - (\mathrm{i}\omega_{32}+\gamma_{32})\rho_{32}, && (9)\\
\dot{\rho_{12}} &= -\mathrm{i}\,(V_2\rho_{14} - \rho_{42}V_1^*) - (\mathrm{i}\omega_{12}+\gamma_{12})\rho_{12}. && (10)
\end{aligned}$$

These equations are governed by $\rho_{ij} = \rho_{ji}^*$ and the closed condition $\rho_{44} + \rho_{33} + \rho_{22} + \rho_{11} = 1$. The decay rates between the three low energy levels are small and the same, $\Gamma_{ij} = \Gamma_0$, $i, j = 1, 2, 3$ $(i \neq j)$. There are $\gamma_{31} = \gamma_{32} = \gamma_{12} = \gamma_0 = 2\Gamma_0$, $\gamma_{43} = \gamma_{41} = \gamma_{42} = \gamma = (3\Gamma + 2\Gamma_0)/2$, and $\Gamma_{43} = \Gamma_{41} = \Gamma_{42} = \Gamma$.

We treat the driving and coupled fields to all orders in V_1, V_2 and V_3, and treat the probe fields to the first order in V_{p_1} and V_{p_2}. In the steady state, the elements of the density matrix are expressed as the terms of Fourier amplitudes. Each Fourier amplitude can be used to represent a photonic process. For example, the first-order term $\rho_{41}(\omega_{p_1})$ represents the absorption spectrum and dispersion of the probe field ω_{p_1}; the third-order term $\rho_{41}(2\omega_1 - \omega_{p_1})$ means an FWM process from the transition $|1\rangle$–$|4\rangle$, where the atom in the state $|1\rangle$ absorbs an ω_1 photon to $|4\rangle$ and simultaneously emits an ω_{p_1} photon to

the state $|1\rangle$ and absorbs an ω_1 photon back to $|4\rangle$. Considering various photonic processes, we express ρ_{ij} in terms of the Fourier amplitudes as follows:

$$\begin{aligned}\rho_{ii} &= \rho_{ii}^{\rm dc}+\rho_{ii}(\omega_1-\omega_{\rm p_1})\,{\rm e}^{-{\rm i}(\omega_1-\omega_{\rm p_1})t}\\ &\quad+\rho_{ii}(\omega_{\rm p_1}-\omega_1)\,{\rm e}^{-{\rm i}(\omega_{\rm p_1}-\omega_1)t}\\ &\quad+\rho_{ii}(\omega_3-\omega_{\rm p_2})\,{\rm e}^{-{\rm i}(\omega_3-\omega_{\rm p_2})t}\\ &\quad+\rho_{ii}(\omega_{\rm p_2}-\omega_3)\,{\rm e}^{-{\rm i}(\omega_{\rm p_2}-\omega_3)t} \qquad (11)\end{aligned}$$

with $i=1,2,3,4$;

$$\begin{aligned}\rho_{41} &= \rho_{41}(\omega_1)\,{\rm e}^{-{\rm i}\omega_1 t}+\rho_{41}(\omega_{\rm p_1})\,{\rm e}^{-{\rm i}\omega_{\rm p_1}t}\\ &\quad+\rho_{41}(\omega_1+\omega_3-\omega_{\rm p_2})\,{\rm e}^{-{\rm i}(\omega_1+\omega_3-\omega_{\rm p_2})t}\\ &\quad+\rho_{41}(\omega_1+\omega_{\rm p_2}-\omega_3)\,{\rm e}^{-{\rm i}(\omega_1+\omega_{\rm p_2}-\omega_3)t}\\ &\quad+\rho_{4i}(2\omega_1-\omega_{\rm p_1})\,{\rm e}^{-{\rm i}(2\omega_1-\omega_{\rm p_1})t}, \qquad (12)\\ \rho_{42} &= \rho_{42}(\omega_2)\,{\rm e}^{-{\rm i}\omega_2 t}+\rho_{42}(\omega_2+\omega_1-\omega_{\rm p_1})\,{\rm e}^{-{\rm i}(\omega_2+\omega_1-\omega_{\rm p_1})t}\\ &\quad+\rho_{42}(\omega_2+\omega_{\rm p_1}-\omega_1)\,{\rm e}^{-{\rm i}(\omega_2+\omega_{\rm p_1}-\omega_1)t}\\ &\quad+\rho_{42}(\omega_2+\omega_3-\omega_{\rm p_2})\,{\rm e}^{-{\rm i}(\omega_2+\omega_3-\omega_{\rm p_2})t}\\ &\quad+\rho_{42}(\omega_2+\omega_{\rm p_2}-\omega_3)\,{\rm e}^{-{\rm i}(\omega_2+\omega_{\rm p_2}-\omega_3)t}, \qquad (13)\\ \rho_{43} &= \rho_{43}(\omega_3)\,{\rm e}^{-{\rm i}\omega_3 t}+\rho_{43}(\omega_{\rm p_2})\,{\rm e}^{-{\rm i}\omega_{\rm p_2}t}\\ &\quad+\rho_{43}(\omega_3+\omega_1-\omega_{\rm p_1})\,{\rm e}^{-{\rm i}(\omega_3+\omega_1-\omega_{\rm p_1})t}\\ &\quad+\rho_{43}(\omega_3+\omega_{\rm p_1}-\omega_1)\,{\rm e}^{-{\rm i}(\omega_3+\omega_{\rm p_1}-\omega_1)t}\\ &\quad+\rho_{43}(2\omega_3-\omega_{\rm p_2})\,{\rm e}^{-{\rm i}(2\omega_3-\omega_{\rm p_2})t}, \qquad (14)\\ \rho_{12} &= \rho_{12}(\omega_2-\omega_1)\,{\rm e}^{-{\rm i}(\omega_2-\omega_1)t}+\rho_{12}(\omega_2-\omega_{\rm p_1})\,{\rm e}^{-{\rm i}(\omega_2-\omega_{\rm p_1})t}\\ &\quad+\rho_{12}(\omega_2-2\omega_1+\omega_{\rm p_1})\,{\rm e}^{-{\rm i}(\omega_2-2\omega_1+\omega_{\rm p_1})t}\\ &\quad+\rho_{12}(\omega_2-\omega_1+\omega_3-\omega_{\rm p_2})\,{\rm e}^{-{\rm i}(\omega_2-\omega_1+\omega_3-\omega_{\rm p_2})t}\\ &\quad+\rho_{12}(\omega_2-\omega_1+\omega_{\rm p_2}-\omega_3)\,{\rm e}^{-{\rm i}(\omega_2-\omega_1+\omega_{\rm p_2}-\omega_3)t}, \qquad (15)\\ \rho_{32} &= \rho_{32}(\omega_2-\omega_3)\,{\rm e}^{-{\rm i}(\omega_2-\omega_3)t}+\rho_{32}(\omega_2-\omega_{\rm p_2})\,{\rm e}^{-{\rm i}(\omega_2-\omega_{\rm p_2})t}\\ &\quad+\rho_{32}(\omega_2-2\omega_3+\omega_{\rm p_2})\,{\rm e}^{-{\rm i}(\omega_2-2\omega_3+\omega_{\rm p_2})t}\\ &\quad+\rho_{32}(\omega_2-\omega_3+\omega_1-\omega_{\rm p_1})\,{\rm e}^{-{\rm i}(\omega_2-\omega_3+\omega_1-\omega_{\rm p_1})t}\\ &\quad+\rho_{32}(\omega_2-\omega_3+\omega_{\rm p_1}-\omega_1)\,{\rm e}^{-{\rm i}(\omega_2-\omega_3+\omega_{\rm p_1}-\omega_1)t}, \qquad (16)\\ \rho_{31} &= \rho_{31}^{\rm dc}+\rho_{31}(\omega_1-\omega_3)\,{\rm e}^{-{\rm i}(\omega_1-\omega_3)t}\\ &\quad+\rho_{31}(\omega_1-\omega_{\rm p_2})\,{\rm e}^{-{\rm i}(\omega_1-\omega_{\rm p_2})t}\\ &\quad+\rho_{31}(\omega_{\rm p_1}-\omega_3)\,{\rm e}^{-{\rm i}(\omega_{\rm p_1}-\omega_3)t}\\ &\quad+\rho_{31}(2\omega_1-\omega_3-\omega_{\rm p_1})\,{\rm e}^{-{\rm i}(2\omega_1-\omega_3-\omega_{\rm p_1})t}\\ &\quad+\rho_{31}(\omega_1-2\omega_3+\omega_{\rm p_2})\,{\rm e}^{-{\rm i}(\omega_1-2\omega_3+\omega_{\rm p_2})t}. \qquad (17)\end{aligned}$$

The Fourier amplitudes are governed by the relation $\rho_{ij}(\omega_k)=\rho_{ji}(-\omega_k)^*$. Inserting Eqs. (11)–(17) into Eqs. (1)–(10), we obtain a set of equations for the Fourier amplitudes. In the first stage, the system interacts only with the pump fields so that we can obtain 15 equations in terms of Fourier amplitudes without probe fields. For example, $\rho_{41}(\omega_1)$ and $\rho_{43}(\omega_3)$ have the form

$$\begin{aligned}&[{\rm i}(\omega_i-\omega_{4i})-\gamma_{4i}]\rho_{4i}(\omega_i)-{\rm i}V_i(\rho_{44}-\rho_{ii})^{\rm dc}\\ &+{\rm i}V_j\rho_{ji}(\omega_i-\omega_j)+{\rm i}V_2\rho_{2i}(\omega_i-\omega_2)=0 \qquad (18)\end{aligned}$$

with $i,j=1,3$ $(i\neq j)$. In the second stage, the probe fields are included in the first order and thus we can obtain 60 equations. For example, $\rho_{41}(\omega_{\rm p_1})$ and $\rho_{43}(\omega_{\rm p_2})$ have the form

$$\begin{aligned}&[{\rm i}(\omega_{\rm p_1}-\omega_{41})-\gamma_{41}]\rho_{41}(\omega_{\rm p_1})-{\rm i}V_{\rm p_1}(\rho_{44}-\rho_{11})^{\rm dc}\\ &-{\rm i}V_1[\rho_{44}(\omega_{\rm p_1}-\omega_1)-\rho_{11}(\omega_{\rm p_1}-\omega_1)]\\ &+{\rm i}V_3\rho_{31}(\omega_{\rm p_1}-\omega_3)+{\rm i}V_2\rho_{21}(\omega_{\rm p_1}-\omega_2)=0, \qquad (19)\\ &[{\rm i}(\omega_{\rm p_2}-\omega_{43})-\gamma_{43}]\rho_{43}(\omega_{\rm p_2})-{\rm i}V_{\rm p_2}(\rho_{44}-\rho_{33})^{\rm dc}\\ &-{\rm i}V_3[\rho_{44}(\omega_{\rm p_2}-\omega_3)-\rho_{33}(\omega_{\rm p_2}-\omega_3)]\\ &+{\rm i}V_1\rho_{13}(\omega_{\rm p_2}-\omega_1)+{\rm i}V_2\rho_{23}(\omega_{\rm p_2}-\omega_2)=0. \qquad (20)\end{aligned}$$

All involved equations can be numerically solved. The probe absorption and refraction are proportional to the real and imaginary parts of the susceptibility, i.e., $\chi(\omega_{\rm p})\propto[\mu_{43}\rho_{43}(\omega_{\rm p_2})+\mu_{41}\rho_{41}(\omega_{\rm p_1})]/(V_{\rm p}/\gamma)$. Since both transitions $|3\rangle$–$|4\rangle$ and $|1\rangle$–$|4\rangle$ have the same dipole moment, $\chi(\omega_{\rm p})\propto[\rho_{43}(\omega_{\rm p_2})+\rho_{41}(\omega_{\rm p_1})]/(V_{\rm p}/\gamma)$. The pump–probe detunings are $\delta_1=\omega_{\rm p_1}-\omega_2$ and $\delta_2=\omega_{\rm p_2}-\omega_2$. The FWM spectra of the probe field are proportional to $[|\rho_{41}(2\omega_1-\omega_{\rm p_1})|+|\rho_{43}(2\omega_3-\omega_{\rm p_2})|]/(V_{\rm p}/\gamma)$.

3. Enhancement of FWM due to CHB

For the system with two probe fields, based on the matches between the probe and pump fields, they are related to a total of four sets of Λ-type level systems and two sets of pump–probe two-level systems. In terms of the probe field $V_{\rm p_1}$, two sets of Λ-type systems $|1\rangle$–$|4\rangle$–$|2\rangle$ and $|1\rangle$–$|4\rangle$–$|3\rangle$, as well as a set of $|1\rangle$–$|4\rangle$ pump–probe two-level system are included. With regard to the probe field $V_{\rm p_2}$, two sets of Λ-type systems $|3\rangle$–$|4\rangle$–$|2\rangle$ and $|3\rangle$–$|4\rangle$–$|1\rangle$, as well as a set of $|3\rangle$–$|4\rangle$ pump-probe two-level system are included. The Λ-type system coupled by a pump field and a probe field is associated with two-photon resonance which can result in EIT, while the pump–probe two-level system is related to the Mollow absorption or the CHB effect and even two-photon gain. The sites of the transparency windows in the absorption spectra, whether arising from EIT or CHB, are related to both the detunings of the pump fields and the coordinate origin of the probe detuning. In this paper, the coordinate origin of the two probe detunings is the level $|2\rangle$, so their resonances are at the detuning of $\delta=\omega_{21}$ and $\delta=\omega_{23}$, respectively. From the perspective of a single field, each probe field is connected with three transparent windows, including two EITs and a hole burning. While each coupled field is connected with two transparent windows, including an EIT and a CHB.

To ensure that the theoretical results can be verified experimentally, the values of the parameters in the Bloch equations should be generally achievable. We define $\Gamma=1.0$ and $\Gamma_0=0.01$, referred to Ref. [41]. Here the Zeeman splitting ω_{31} between $M_{Fg}=3$ and $M_{Fg}=1$ is set to 10.0, so that $\omega_{32}=\omega_{21}=5$. To satisfy the probe Rabi frequencies

$2|V_{p_1}|$ and $2|V_{p_2}|$ are much smaller than the driving Rabi frequency $2|V_2|$, coupled Rabi frequencies $2|V_1|$ and $2|V_3|$, we set $|V_{p_1}| = |V_{p_2}| = 0.001$, and $|V_i| \geq 0.1$, $i = 1,2,3$. In this paper, considering the symmetry of absorption spectra, we always set the driving detuning $\Delta_2 = 0$.

Since the linear absorption spectra can reflect various optical effects and their sites, to study the FWM we take the linear absorption spectra as a reference. In Figs. 2 and 3, the detunings of the coupled fields is set as $\Delta_1 = -5$ and $\Delta_3 = 5$. Figure 2 illustrates the linear response (including absorption spectra and dispersion) and the corresponding FWM spectra in two different coupled Rabi frequencies. In the absorption spectra, as shown in Figs. 2(a) and 2(c), there are two sets of EITs linked with the driving field whose transparent windows are located at $\delta = \pm 5$, while the width of the transparent window is as large as $2V_2 = 10$. There are also two sets of EITs linked with two coupled fields whose dips are located at $\delta = \pm 10$. The one at $\delta = -10$ is the match between the probe field V_{p_2} and the coupled field V_1, while the other at $\delta = 10$ is the match between the probe field V_{p_1} and the coupled field V_3. However, the dip at $\delta = 0$ corresponds to two sets of overlapped CHBs. One comes from the match between the probe field V_{p_1} and the coupled field V_1, and the other comes from the match between the probe field V_{p_2} and the coupled field V_3. In the FWM spectra illustrated in Figs. 2(b) and 2(d), there is a single FWM signal at $\delta = 0$, which shows a sharp peak at $V_1 = V_3 = 0.1$ and an enhancement in magnitude and width at $V_1 = V_3 = 0.7$. From the previous analysis, this isolated FWM signal corresponds to a pair of overlapped CHBs. In contrast, the FWM response of EITs at $\delta = \pm 10$ can be neglected in front of CHB.

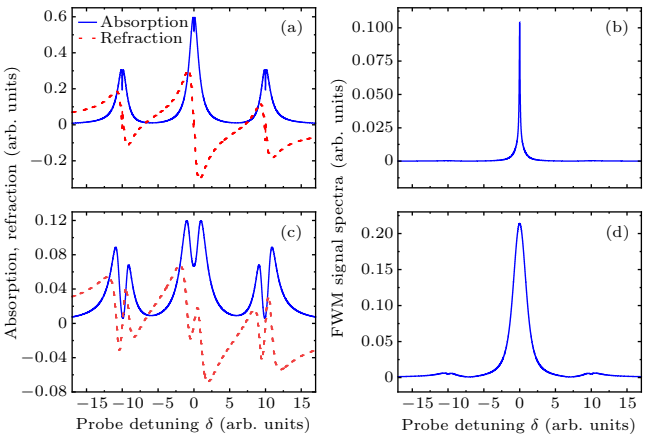


Fig. 2. Linear responses and the corresponding FWM spectra. (a) Linear absorption spectrum and dispersion with $V_1 = V_3 = 0.1$ and (b) the corresponding FWM spectrum; (c) linear absorption spectrum and dispersion with $V_1 = V_3 = 0.7$ and (d) the corresponding FWM spectrum. The common parameters are $V_2 = 5$, $\Delta_1 = -5$ and $\Delta_3 = 5$.

In the following, on the contrary, the coupled Rabi frequencies are fixed at $V_1 = V_3 = 2.5$, while the driving Rabi frequency varies. Figure 3 illustrates the linear responses and the corresponding FWM spectra in different driving Rabi frequencies. Since the coupled detunings are maintained, the sites of EITs and CHBs in the absorption spectra are the same as those in Fig. 2. It is clear that the two FWM spectra exhibit a multi-peak structure, where the three-peak FWM spectra at the site $\delta = 0$ correspond to the two overlapped CHBs. In the three-peak FWM, the gap between the central peak and one side peak is equivalent to the absolute value of the coupled detunings. The magnitude of the central peak is greater than those of the peaks on both sides owing to inherent characteristics of CHB under the coupled detunings.[24] Since the small driving Rabi frequency in the EIT corresponds to a large quantum coherence, $V_2 = 0.1$ can lead to a pronounced nonlinear response. When $V_2 = 0.1$, the EITs located at $\delta = \pm 5$ correspond to an FWM that is much larger than the FWM from the EITs at $\delta = \pm 10$, but still smaller than the FWM due to the CHB at $\delta = 0$, as shown in Fig. 3(b).

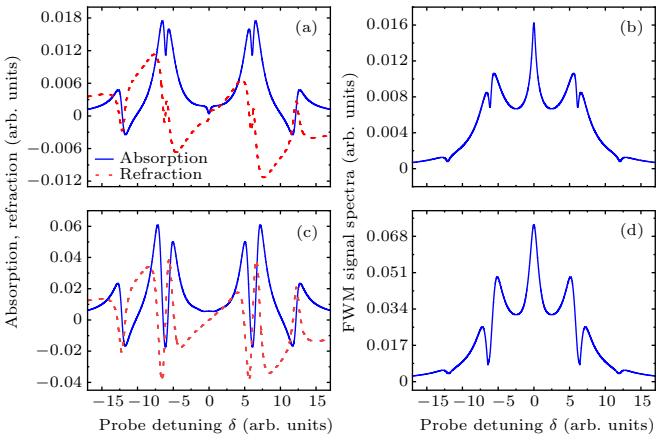


Fig. 3. Linear responses and the corresponding FWM spectra. (a) Linear absorption spectrum and dispersion with $V_2 = 0.1$ and (b) the corresponding FWM spectrum; (c) linear absorption spectrum and dispersion with $V_2 = 1$ and (d) the corresponding FWM spectrum. The common parameters are $V_1 = V_3 = 2.5$, $\Delta_1 = -5$ and $\Delta_3 = 5$.

However, the magnitude of FWM is enhanced with the increase of the driving Rabi frequency. This enhancement is related to the dominant role of CHB. Due to the effect of pumping, the increasing driving Rabi frequency results in the increasing population on the levels $|1\rangle$ and $|3\rangle$, and thus strengthens the CHB effect. This figure also illustrates that the CHB plays a key role in the FWM spectra.

Subsequently, in Figs. 4 and 5 the detunings of the coupled fields are set as $\Delta_1 = -2.5$ and $\Delta_3 = 2.5$. Figure 4 illustrates the linear responses and corresponding FWM spectra in different coupled Rabi frequencies. As the coupled Rabi frequencies $V_1 = V_3 = 0.1$, it can be inferred from the absorption spectrum that at $\delta = \pm 5$, there are two sets of EITs linked with the driving field, which have wide transparent windows due to $V_2 = 2.5$. While, at $\delta = \pm 7.5$, there are also two sets of EITs related to the coupled fields. The one at $\delta = -7.5$ comes from the match between the probe field V_{p_2} and the coupled

field V_1, while the other at $\delta = 7.5$ comes from the match between the probe field V_{p_1} and the coupled field V_3. It is noted that the dips at $\delta = \pm 2.5$ correspond to two sets of CHBs. One builds from the match between the probe field V_{p_1} and the coupled field V_1, and the other builds from the match between the probe field V_{p_2} and the coupled field V_3. As the coupled Rabi frequencies increase, the dips at $\delta = \pm 2.5$ and $\delta = \pm 7.5$ become broadened and deeper, as shown in Fig. 4(c). The FWM spectra are straight and simple, showing that there are two big peaks at $\delta = \pm 2.5$, which correspond to two CHBs. There are also two small dips at $\delta = \pm 7.5$ linked with EITs, but they can be neglected compared with the two primary peaks.

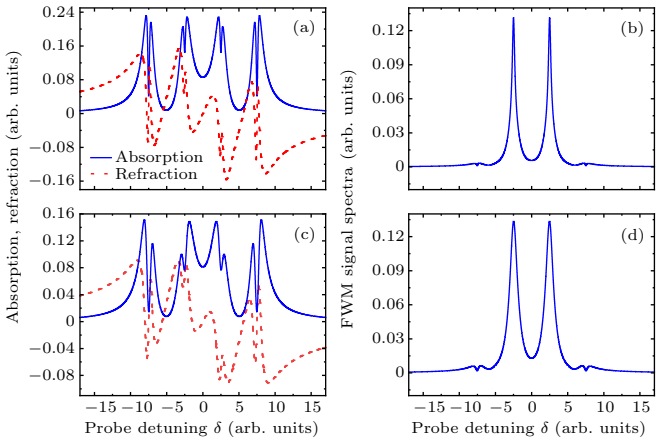


Fig. 4. Linear responses and the corresponding FWM spectra. (a) Linear absorption spectrum and dispersion with $V_1 = V_3 = 0.3$ and (b) the corresponding FWM spectrum; (c) linear absorption spectrum and dispersion with $V_1 = V_3 = 0.5$ and (d) the corresponding FWM spectrum. The common parameters are $V_2 = 2.5$, $\Delta_1 = -2.5$ and $\Delta_3 = 2.5$.

Then the coupled Rabi frequencies are fixed while the driving Rabi frequency varies. Figure 5 illustrates the linear responses and corresponding FWM spectra in different driving Rabi frequencies under the coupled Rabi frequencies $V_1 = V_3 = 1$. Since the detunings of the driving and coupled fields are identical to Fig. 4, the sites of EITs and CHBs are maintained in the absorption spectra, as illustrated in Fig. 5(a). When the driving Rabi frequency increases to $V_2 = 5$, the transparent windows at $\delta = \pm 5$ become broader, as shown in Fig. 5(c). As far as the FWM signal is concerned, a CHB still corresponds to an FWM spectrum with three-peak structure, whose central peak is larger than the peaks on both sides. So the largest FWM signal at $\delta = \pm 2.5$ comes from the CHB, while the peak at $\delta = 0$ originates from the superposition of two side peaks from either of three-peak probe FWM spectra, as shown in Fig. 5(b). So in some cases the peak at $\delta = 0$ can exceed the peaks at $\delta = \pm 2.5$ due to the superposition, as shown in Fig. 5(d). In contrast, the FWM signal corresponding to the EITs at $\delta = \pm 5$ and $\delta = \pm 7.5$ can still be neglected in front of CHB. It can be seen that the FWM magnitudes at $\delta = \pm 5$ are covered by the three-peak constructure of FWM spectra from CHBs. Additionally, it can be seen that the FWM magnitude at $V_2 = 5$ is smaller than the FWM magnitude at $V_2 = 0.5$. The reduction is relevant to the saturation effect, where the levels $|2\rangle$ and $|4\rangle$ suffer from the Autler–Towns (A-T) splitting, which takes the CHB effect to the saturated state, thereby resulting in a reduction in the magnitude of FWM. It is noted that, in the saturation state, FWM spectra with seven or nine peaks can be obtained in terms of the dressed-state theory.[36] In this figure, the FWM spectra with seven peaks is achieved.

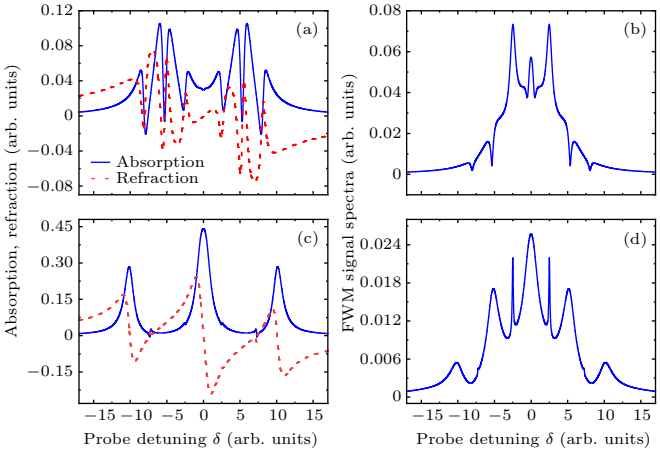


Fig. 5. Linear responses and the corresponding FWM spectra. (a) Linear absorption spectrum and dispersion with $V_2 = 0.5$ and (b) the corresponding FWM spectrum; (c) linear absorption spectrum and dispersion with $V_2 = 5$ and (d) the corresponding FWM spectrum. The common parameters are $V_1 = V_3 = 1$, $\Delta_1 = -2.5$ and $\Delta_3 = 2.5$.

In the above content, the FWM spectra corresponding to the overlap of two CHBs and the single CHB are included. Below, we analyze the FWM spectra in the state of overlapped CHB and EIT. Figure 6 illustrates the linear responses and relevant FWM spectra in different coupled Rabi frequencies. In Figs. 6(a)–6(d), the coupled detunings are set as $\Delta_1 = \Delta_3 = 5$. The transparent windows at $\delta = \pm 5$ correspond to two sets of EITS linked with the driving field. The dips at $\delta = 0$ and $\delta = 10$ both correspond to overlapped CHB and EIT. Individually, the CHB at $\delta = 0$ refers to the match between the probe field V_{p_2} and the coupled field V_3, and the EIT at $\delta = 0$ refers to the match between the probe field V_{p_2} and the coupled field V_1. While, the CHB at $\delta = 10$ refers to the match between the probe field V_{p_1} and the coupled field V_1, and the EIT at $\delta = 10$ refers to the match between the probe field V_{p_1} and the coupled field V_3. As $V_1 = V_3 = 0.1$, it is clear that two sharp FWM peaks with equal magnitude emerge at $\delta = 0$ and $\delta = 10$, as illustrated in Fig. 6(b). As $V_1 = V_3 = 0.5$, the dips in the linear absorption spectrum at $\delta = 0$ and $\delta = 10$ become more pronounced, as illustrated in Fig. 6(c). However, the magnitude of the FWM signal becomes smaller while the single peak is replaced by two peaks, as illustrated in Fig. 6(d). Here we attribute the reduction of the magnitude of FWM signal to the A-T splitting effect.

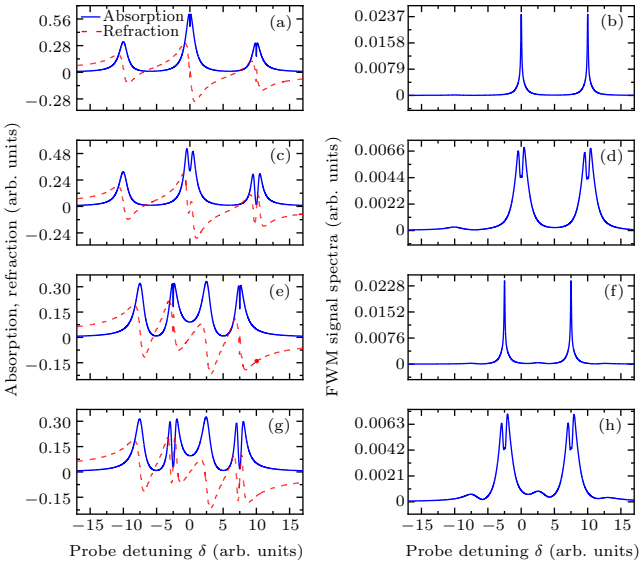


Fig. 6. Linear responses and the corresponding FWM spectra. (a) Linear absorption spectrum and dispersion with $V_1 = V_3 = 0.1$ and (b) the corresponding FWM spectrum; (c) linear absorption spectrum and dispersion with $V_1 = V_3 = 0.5$ and (d) the corresponding FWM spectrum; their common parameters are $V_2 = 5$, $\Delta_1 = 5$ and $\Delta_3 = 5$. (e) Linear absorption spectrum and dispersion with $V_1 = V_3 = 0.1$ and (f) the corresponding FWM spectrum; (g) linear absorption spectrum and dispersion with $V_1 = V_3 = 0.5$ and (h) the corresponding FWM spectrum; their common parameters are $V_2 = 2.5$, $\Delta_1 = 2.5$ and $\Delta_3 = 2.5$.

In Figs. 6(e)–6(h), the coupled detunings become $\Delta_1 = \Delta_3 = 2.5$. Similarly, the transparent windows at $\delta = \pm 5$ are the EITs related to the driving field V_2. The dips at $\delta = -2.5$ and $\delta = 7.5$ both correspond to overlapped CHB and EIT. Individually, the CHB at $\delta = -2.5$ refers to the match between the probe field V_{p_2} and the coupled field V_3, and the EIT at $\delta = -2.5$ refers to the match between the probe field V_{p_2} and the coupled field V_1. The CHB at $\delta = 7.5$ refers to the match between the probe field V_{p_1} and the coupled field V_1, and the EIT at $\delta = 7.5$ refers to the match between the probe field V_{p_1} and the coupled field V_3. Therefore, under the same coupled Rabi frequencies, their FWM spectra have exactly the same performances compared with the previous example in Figs. 6(a)–6(d). Compared with other states of CHB, the magnitude of FWM in the state of overlapped CHB and EIT is nearly one tenth of that in the state of two overlapped CHBs. It indicates that both the EIT and A-T splitting weaken the nonlinear response of the FWM and bring the magnitude of the FWM down.

Similarly, the coupled detunings remain $\Delta_1 = \Delta_3 = 2.5$, but the coupled Rabi frequencies are fixed at $V_1 = V_3 = 0.5$, and the driving Rabi frequency V_2 varies. The impact of the driving field on FWM spectra is examined, as shown in Fig. 7. Since the couple detunings remain, the sites of EITs and CHBs in the absorption spectra are maintained with Figs. 6(e)–6(h). At $V_2 = 0.1$, it was observed that the FWM peaks appear at the sites where the CHBs are occurring, as illustrated in Fig. 7(b). At $V_2 = 2.5$, either of the single peaks is split into double peaks due to the A-T splitting developed from the EIT, as illustrated in Fig. 7(d). At $V_2 = 5$, owing to the interaction between EITs and CHBs, a subnatural-linewidth FWM peak is formed, as shown in Fig. 7(f). From a comparison of the three cases, it can be seen that their FWM magnitudes scarcely change at all, but they remain at a very low magnitude.

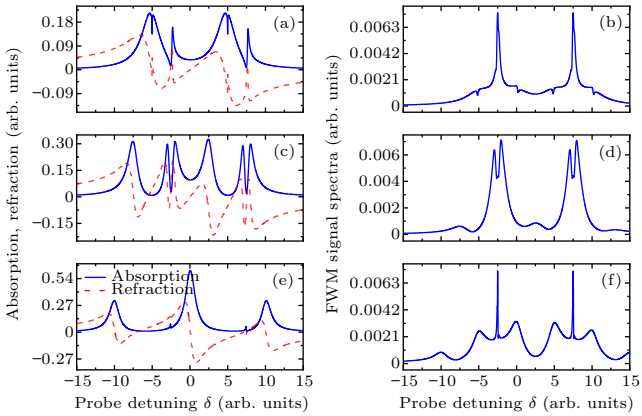


Fig. 7. Linear responses and the corresponding FWM spectra. (a) Linear absorption spectrum and dispersion with $V_2 = 0.1$ and (b) the corresponding FWM spectrum; (c) linear absorption spectrum and dispersion with $V_2 = 2.5$ and (d) the corresponding FWM spectrum; (e) linear absorption spectrum and dispersion with $V_2 = 5.0$ and (f) the corresponding FWM spectrum. The common parameters are $V_1 = V_3 = 0.5$, $\Delta_1 = 2.5$ and $\Delta_3 = 2.5$.

In the following, we analyze the EIAs and their corresponding FWM spectra. Figure 8 illustrates the double EIAs in an absorption spectrum and corresponding FWM spectra. In this figure, since the coupled detunings are identical to those in Fig. 7, the sites of EITs and CHBs in the absorption spectra are similar to those in Fig. 7. However, with the increase of the Rabi frequencies, owing to the interaction between EITs, the subnatural-linewidth absorption of EIA comes into being between the neighboring EITs. Individually, the origin of the subnatural-linewidth absorption in positive probe detuning comes from the interaction between two EITs (the one is from the match of V_{p_1} and V_2, and the other is from the match of V_{p_1} and V_3). While, the origin of the subnatural-linewidth absorption in negative probe detuning comes from the interaction between the other two EITs (the one is from the match of V_{p_2} and V_2, and the other is from the match of V_{p_2} and V_1). As $V_1 = V_2 = V_3 = 5$, the absorption peak with subnatural linewidth does not overlap with the normal absorption peak, so the enhanced absorption does not arrive, as shown in Fig. 8(a). While, as $V_1 = V_2 = V_3 = 5.7$, the absorption peak with subnatural linewidth overlaps with the normal absorption peak, and thus the two enhanced atomic absorption peaks (double EIAs) come into being, as shown in Fig. 8(c). Under similar parameters, the involvement of EIA makes the magnitude of the FWM signal increase to a certain degree. However, owing to the participation of the effect of A-T splitting, the magnitude of the FWM is still far smaller than that of single CHB or the overlapped CHBs.

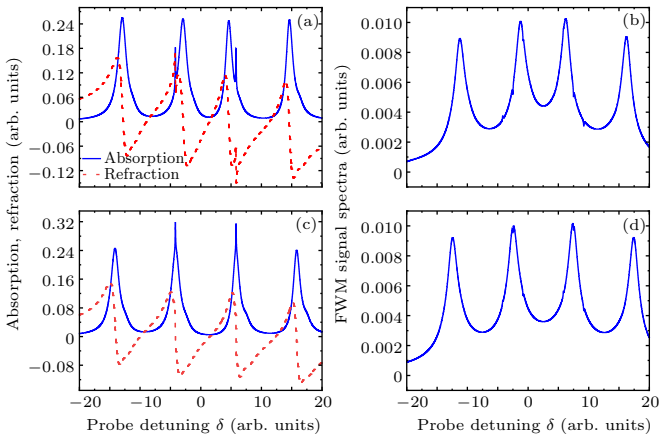


Fig. 8. Linear responses and the corresponding FWM spectra. (a) Linear absorption spectrum and dispersion with $V_1 = V_2 = V_3 = 5$ and (b) the corresponding FWM spectrum; (c) linear absorption spectrum and dispersion with $V_1 = V_2 = V_3 = 5.7$ and (d) the corresponding FWM spectrum. The common parameters are $\Delta_1 = 2.5$ and $\Delta_3 = 2.5$.

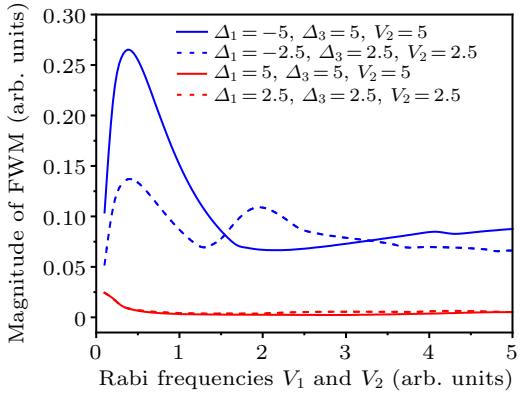


Fig. 9. The magnitude of FWM signal versus the coupled Rabi frequencies ($V_1 = V_3$). The solid blue line ($\Delta_1 = -5$, $\Delta_3 = 5$ and $V_2 = 5$) corresponds to the overlapped CHBs, while the dotted blue line ($\Delta_1 = -2.5$, $\Delta_3 = 2.5$ and $V_2 = 2.5$) corresponds to the single CHB, and the red lines correspond to the overlapped EIT and CHB.

In this coherent system, the CHB has a significant effect on the enhancement of FWM. In this paper, the three states of CHB are involved and they are the overlapped CHBs, the single CHB and the overlapped EIT and CHB. Figure 9 illustrates the FWM magnitude versus the coupled Rabi frequencies. As the coupled detunings are $\Delta_1 = -5$ and $\Delta_3 = 5$, it corresponds to the state of overlapped CHB. As the coupled detunings are $\Delta_1 = -2.5$ and $\Delta_3 = 2.5$, it corresponds to the state of a single CHB. However, as the coupled detunings are $\Delta_1 = 5$ and $\Delta_3 = 5$, or $\Delta_1 = 2.5$ and $\Delta_3 = 2.5$, it corresponds to the state of overlapped CHB and EIT. From a comparison between the three states, the state of overlapped CHBs corresponds to the largest FWM magnitude, followed by the state of a single CHB, whose FWM magnitude is about half of the magnitude of the first state of CHB. The state of overlapped CHB and EIT corresponds to the smallest FWM magnitude, which is only no more than one tenth of the magnitude of the first state of CHB. The FWM magnitude in the initial stage exhibits growth for the first two states of CHB and shows a reduction for the third state of CHB. The reduction in the state of overlapped CHB and EIT is obviously related to the performance of the A-T splitting developed from the EIT, because the nonlinear response in a pure EIT system drops with the increase of coupled Rabi frequency.

4. Conclusion

We have theoretically explored the FWM spectra of a special degenerate two-level atomic system whose upper level has $F_e = 0$ and lower level has $F_g = 1$. With a magnetic field, it develops into a tripod-type four-level atomic system, to which three pump and two probe fields are applied. According to the match between the probe and pump fields, this atom–light system can form four sets of EITs and two sets of CHBs. When using detuned coupling fields, we can obtain diverse absorption spectra including double EIAs. According to the absorption spectra, the positions of EITs and CHBs in the absorption spectrum can be marked. On this basis, we study the corresponding FWM signal spectra. In the same parameters, we have found that CHBs have far larger FWM responses than EITs. There are three states for the CHB in the FWM spectra. From the comparison among the three states, the overlapped state of two CHBs corresponds to the largest FWM magnitude. For the state of a single CHB, the corresponding FWM signal has decreased, whose FWM magnitude is about half of the state of the overlapped CHBs. However, for the overlapped state of a CHB and an EIT, the corresponding FWM signal has a greater drop, whose magnitude is only no more than one tenth that of the overlapped double CHBs. Finally, we have examined the FWM response of double EIAs of the system and found that the magnitude of FWM is enhanced with the EIAs.

Acknowledgement

Project supported by the Open Subject of the State Key Laboratory of Quantum Optics and Quantum Optics Devices (Grant No. KF202209).

References

[1] Lin Y H and Lin G R 2013 *Laser Physics Letters* **10** 045109
[2] Liu J and Kobayashi T 2010 *Sensors* **10** 4296
[3] Qiu M W, Cai C Q and Zhang Z X 2022 *Chin. Phys. B* **31** 104207
[4] Zhou X, Li Z, Zhou Y, Bi M, Hu M, Yang G, Li Q, Lu Y and Wang T 2019 *Optical and Quantum Electronics* **51** 297
[5] Trofimov V A and Kuchik L E 2017 *Laser Application in Microelectronic and optoelectronic Manufacturing (LAMOM) XXII* **10091** 31
[6] Dorfman K, Liu S, Lou Y, Wei T, Jing J, Schlawin F and Mukamel S 2021 *Proc. Natl. Acad. Sci. USA* **118** e2105601118
[7] Li J, Zeng J, Li F, Zhang Y and Cai Y 2022 *Opt. Express* **30** 39762
[8] Lou Y, Chen Y, Wang J, Liu S and Jing J 2023 *Science China Physics, Mechanics & Astronomy* **66** 250311
[9] Feng L T, Cheng Y J, Qi X Z, Zhou Z Y, Zhang M, Dai D X, Guo G C and Ren X F 2023 *Optica* **10** 702
[10] Muller M, Bounouar S, Jons K D, Glassl M and Michler P 2014 *Nat. Photonics* **8** 224

[11] Zhang K, Wang W, Liu S, Pan X, Du J, Lou Y, Yu S, Lv S, Treps N, Fabre C et al. 2020 *Phys. Rev. Lett.* **124** 090501
[12] Pan C, Li H, Pang H, Ru R, Zhang S, Wei D, Chen H, Gao H and Li F 2023 *Laser & Photonics Reviews* **18** 2300625
[13] Qin Z, Gao L and Jing J 2015 *Appl. Phys. Lett.* **106** 211104
[14] Pan X, Chen H, Wei T, Zhang J, Marino A M, Treps N, Glasser and Jing J 2018 *Phys. Rev. B* **97** 161115
[15] Lipsich A, Barreiro S, Akulshin A and Lezama A 2000 *Phys. Rev. A* **61** 053803
[16] Mollow B 1972 *Phys. Rev. A* **5** 2217
[17] Harris H E, Field G and Imamoglu. A 1990 *Phys. Rev. Lett.* **64** 1107
[18] Boller, K J, Imamoglu A and Harris S E 1991 *Phys. Rev. Lett.* **66** 2593
[19] Gea-Banacloche J, Li Y Q, Jin S Z and Xiao M 1995 *Phys. Rev. A* **51** 576
[20] Arimondo E 1996 *Progress in Optics* **35** 257
[21] Gray H, Whitley R and Stroud C 1978 *Opt. Lett.* **3** 218
[22] Alzetta G, Gozzini A, Moi L and Orriols G 1976 *Nuovo Cimento B* **36** 5
[23] Taichenachev A, Tumaikin A and Yudin V 1999 *Phys. Rev. A* **61** 011802
[24] Renzoni F, Cartaleva S, Alzetta G and Arimondo E 2001 *Phys. Rev. A* **63** 065401
[25] Boyd R W, Raymer M G, Narum P and Harter D J 1981 *Phys. Rev. A* **24** 411
[26] Hillman L W, Boyd R W, Krasinski J and Stroud C 1983 *Opt. Commun.* **45** 416
[27] Shah V, Knappe S, Hollberg L and Kitching J 2007 *Opt. Lett.* **32** 1244
[28] Lu Y, Zhang J Q, Cui J M, Cao D Y, Zhang S, Huang Y F, Li C F and Guo G C 2015 *Phys. Rev. A* **92** 023420
[29] Lin G W, Yang J, Niu Y P and Gong S Q 2015 *Chin. Phys. B* **25** 014201
[30] Selvan K 2018 *Euro. Phys. J. D* **72** 1
[31] Kang H and Zhu Y 2003 *Phys. Rev. Lett.* **91** 093601
[32] Zhang Y, Brown A W and Xiao M 2007 *Phys. Rev. Lett.* **99** 123603
[33] Pritchard J D, Maxwell D, Gauguet A, Weatherill K J, Jones M and Adams C S 2010 *Phys. Rev. Lett.* **105** 193603
[34] Stanojevic J, Grangier P and Cote R 2016 *J. Phys. B: Atom. Mol. Opt. Phys.* **49** 124003
[35] Glorieux Q, Dubessay R, Guibal S, Guidoni L, Likforman J P, Coudreau T and Arimondo E 2010 *Phys. Rev. A* **82** 033819
[36] Sun Q, Gu Y and Gong Q 2006 *Journal of Modern Optics* **53** 1663
[37] Barkov L, Melik-Pashayev D and Zolotorev M 1989 *Opt. Commun.* **70** 467
[38] Diddams S A, Diels J C and Atherton B 1998 *Phys. Rev. A* **58** 2252
[39] Bergmann K, Theuer H and Shore B 1998 *Rev. Mod. Phys.* **70** 1003
[40] Gerez P and Hartmann F 1977 *IEEE Journal of Quantum Electronics* **13** 344
[41] Windholz L 2001 *Physica Scripta* **2001** 81